Structural and photoluminescence properties of porous GaP formed by electrochemical etching

Katsuhiro Tomioka and Sadao Adachi[a)]

Department of Electronic Engineering, Faculty of Engineering, Gunma University, Kiryu-shi, Gunma 376-8515, Japan

(Received 27 May 2005; accepted 29 August 2005; published online 5 October 2005)

The structural and optical properties of porous GaP have been studied by scanning electron microscopy, spectroscopic ellipsometry, and photoluminescence (PL) spectroscopy. Porous GaP layers were fabricated by anodic etching in $HF:H_2O:C_2H_5OH=1:1:2$ electrolyte on *n*-type (100) and (111)*A* substrates. The morphology of the porous GaP layer is found to depend strongly on the surface orientation. Apart from the red emission band at ~1.7 eV, a supra-band-gap (E_g^X) emission has been clearly observed on the porous GaP (111)*A* sample. The anodic porous layer on the (100) substrate, on the other hand, has shown only the red emission at 300 K and both red and green donor-acceptor pair emissions at low temperatures. The correlation between the PL properties and the porous morphology is discussed. An optical transition model is also proposed for the explanation of the PL emission properties of the porous GaP samples. © *2005 American Institute of Physics*. [DOI: 10.1063/1.2076445]

I. INTRODUCTION

Porous semiconductors have received much attention since the observation of visible room-temperature luminescence from porous silicon.[1] The anodic technique has been used for several decades now and has proved to be a useful nanofabrication tool in the synthesis of porous structures.[2–4] Like silicon, compound semiconductors such as GaP and GaAs have been investigated in the form of porous structures and many different properties relative to those of bulk materials have been reported. For instance, UV and visible emissions have been observed in the porous layers of GaP,[5–7] GaAs,[8,9] and InP.[10–12] Stable field electron emitters have been fabricated using porous GaP and GaAs layers.[13,14] A large birefringence has also been observed in porous GaP and InP, allowing phase matching for second-harmonic generation.[15]

Our aim in this paper is to present data concerning the structural and optical properties of porous GaP formed on (100) and (111)*A* substrates by anodic etching. In silicon,[3,16] the pores tend to grow in ⟨100⟩ directions. With increasing anodic voltage, the ⟨100⟩ directions become more dominating for the side pores as well. The pore formation in silicon is, therefore, an anisotropic process. Various *n*-type compound semiconductors have also been fabricated as porous structures on (100) substrates by electrochemical etching. No surface orientation dependence has, however, been considered in these studies. Here, we form porous structures not only on the (100) substrate, but also on the (111)*A* substrate and compare their structural and optical properties by a scanning electron microscopy (SEM), spectroscopic ellipsometry (SE), and photoluminescence (PL) spectroscopy. An interband transition model is proposed for the explanation of PL emission properties in anodically formed porous GaP samples.

a)Electronic mail: adachi@el.gunma-u.ac.jp

II. EXPERIMENT

The samples used in this study were *n*-type, sulfur-doped GaP with (100) and (111)*A* surface orientations. They were doped with a sulfur donor density of $\sim 3\times10^{17}$ cm^{-3}. The porous layers were fabricated by anodic etching of GaP wafers in an electrochemical cell. The electrolyte used was a 46% solution of HF in deionized water and methanol with a volume ratio of $HF:H_2O:C_2H_5OH=1:1:2$. The etching process was performed by illuminating a light from a 100 W xenon lamp at room temperature for $t=10$, 30, and 60 min at a current density of 20 mA/cm^2.

The anodized GaP layer was evaluated by SEM. The automatic ellipsometer was of the polarizer-sample-rotating-analyzer type (DVA-36VW-A, Mizojiri Optical). A 150 W xenon lamp was used as a light source. The SE measurements were carried out in the 1.5–5.4 eV photon-energy range at room temperature. The angles of incidence and polarizer azimuth were set at 45° and 40°, respectively.

PL measurements were performed using a grating spectrometer (Jasco CT-25C) and a Peltier-device-cooled photomultiplier tube (Hamamatsu R375). The 325 nm line of a He–Cd laser (Kimmon IK3302R-E) chopped at 328 Hz was used as the excitation light source. The measurements were performed using a closed-cycle refrigerator cryostat (Iwatani CRT105PL) at $T=15-300$ K.

III. RESULTS AND DISCUSSION

A. Scanning electron microscopy observation

We show, in Figs. 1 and 2, SEM images of the porous GaP layer formed on the (100) substrate by anodic etching for $t=10$ and 30 min, respectively. The SEM images of a porous GaP formed on the (111)*A* substrate for $t=30$ min are also shown in Fig. 3. In accordance with these SEM images, we depict in Figs. 4(a)–4(h) the possible anodic etching processes on the GaP (100) and (111)*A* substrates, respectively.

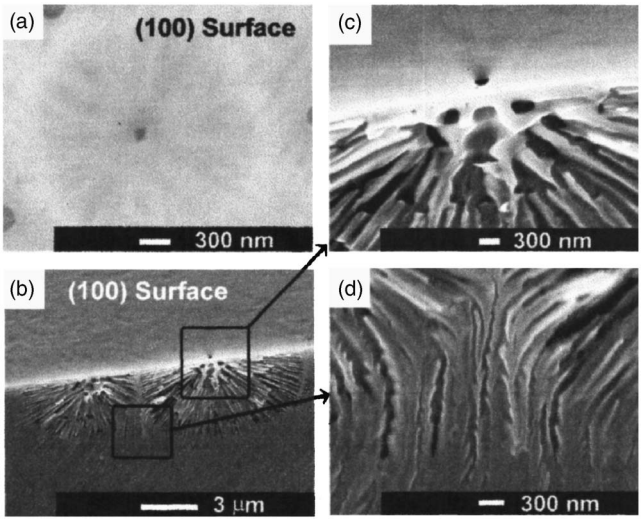

FIG. 1. Top and cross-sectional SEM images of porous GaP (100) sample formed anodically in $HF:H_2O_2:C_2H_5OH=1:1:2$ electrolyte for $t=10$ min at a constant current of 20 mA/cm^2.

At the beginning of the GaP (100) process, the etching starts at surface imperfections [Fig. 4(a)].[17,18] After initial pitting of the surface, further etching proceeds in all directions radically away from the initial surface imperfection [Figs. 4(b) and 4(c)]. As a result, a porous domain is formed around each etch pit. The pores in each domain distinctly grow perpendicular to the equipotential lines of the electric field in the anodized specimen. Since the etching proceeds at the same rate in all directions, the boundary of the porous region, that is, the porous domain, is circular, as clearly seen in Fig. 1(a) [see also Fig. 1(b)]. Following etching for an extended period, the pores from different domains eventually meet and then change their direction of growth, resulting in nearly vertical walls between neighboring porous domains [Figs. 1(d) and 4(d)]. Finally, the density of porous domains depends on the local density of surface imperfections initiating the formation of radial pores, as seen in Fig. 2(a).

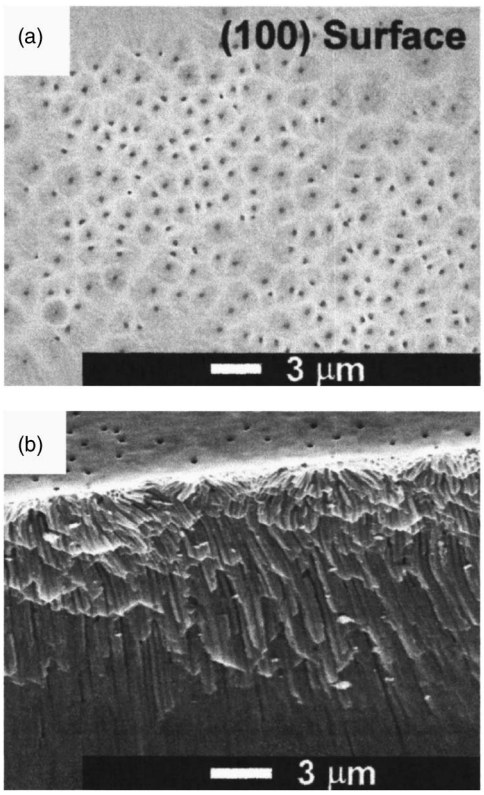

FIG. 2. (a) Top and (b) cross-sectional SEM images of porous GaP (100) sample formed anodically in $HF:H_2O_2:C_2H_5OH=1:1:2$ electrolyte for $t=30$ min at a constant current of 20 mA/cm^2.

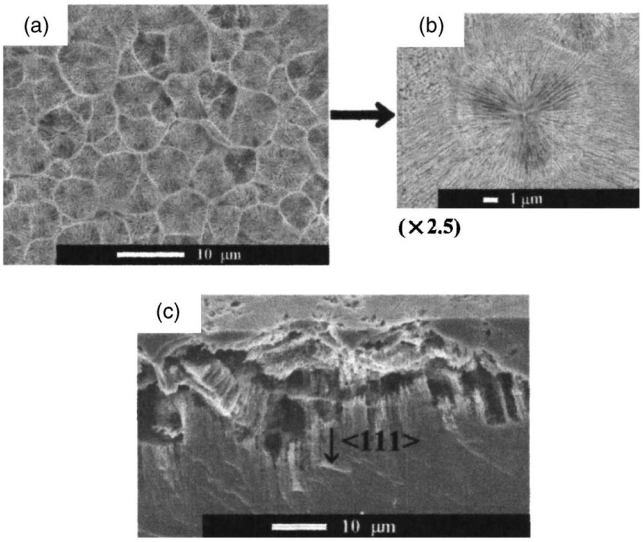

FIG. 3. (a), (b) Top and (c) cross-sectional SEM images of porous GaP (111)*A* sample formed anodically in $HF:H_2O_2:C_2H_5OH=1:1:2$ electrolyte for $t=30$ min at a constant current of 20 mA/cm^2.

In the case of the GaP (111)*A* surface, the anodization leads to a surface layer with a pillar structure characterized by an array of petal-like patterns [Fig. 3(a)]. Each petal-like pattern consists of a lot of columns growing radically and stretching parallel to the (111)*A* surface. The resulting petal-

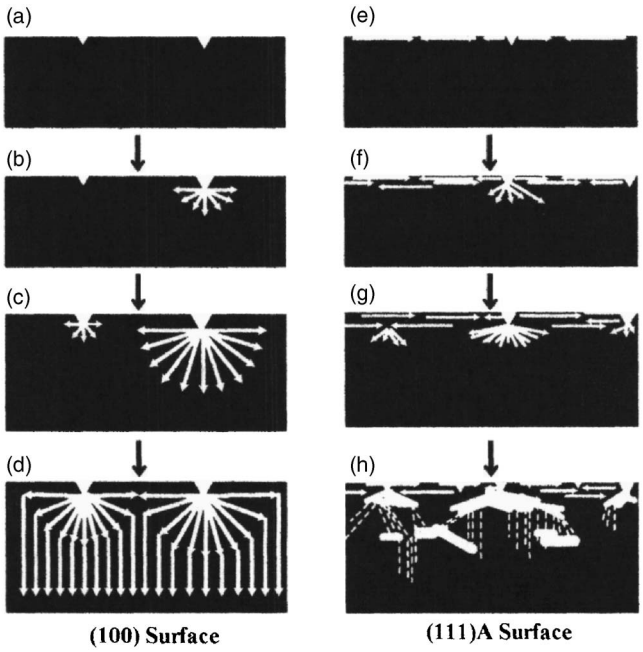

FIG. 4. Possible anodic etching steps of GaP (100) and (111)*A* surfaces formed in $HF:H_2O_2:C_2H_5OH=1:1:2$ electrolyte.

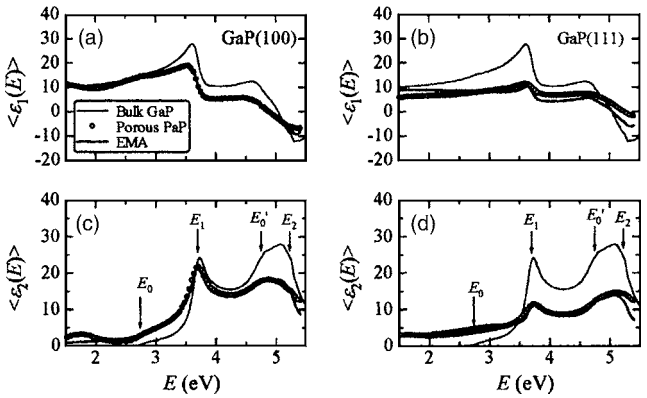

FIG. 5. $\langle\varepsilon(E)\rangle$ spectra for GaP (100) [(a) and (b)] and GaP (111)*A* samples [(c) and (d)] anodically etched in $HF:H_2O_2:C_2H_5OH=1:1:2$ electrolyte for $t=60$ min at constant current of 20 mA/cm^2. For comparison, the $\varepsilon(E)$ spectra for clean, bulk GaP (Ref. 21) are shown by dashed lines. The three-phase LRA-EMA analysis results are also shown by solid lines.

like patterns have a threefold symmetry [Fig. 3(b)]. Further anodization leads to the formation of a beehivelike porous network growing inside the sample [Fig. 3(c)]. Large voids are found to be formed partly in such a beehivelike porous network. Figures 4(e)–4(h) schematically illustrate such anodic etching steps observed on the (111)*A* substrate.

B. Spectroscopic-ellipsometry analysis

SE is a very surface-sensitive technique.[19,20] It entails measuring the ellipsometric variables Ψ and Δ, where Ψ is the change in amplitude ratio and Δ is the change in the phase difference of polarized light upon reflection from a sample surface. Any change in the measured Ψ and Δ reflects a change in the surface conditions, such as adsorbed chemical species, residual film, and surface roughness. The SE measurements therefore yield direct information about the relative quality of surface regions prepared in different ways.

The pseudodielectric function, $\langle\varepsilon(E)\rangle=\langle\varepsilon_1(E)\rangle+i\langle\varepsilon_2(E)\rangle$, is a quantity derived from the SE data using the two-phase (ambient/substrate) model. We show in Fig. 5 the pseudodielectric-function spectra $\langle\varepsilon(E)\rangle$ for GaP (100) and (111)*A* samples anodically etched for $t=60$ min. For comparison, the $\varepsilon(E)$ spectra for clean, bulk GaP (Ref. 21) are shown by dashed lines.

The dielectric function of a crystalline semiconductor is closely related to its energy-band structure, and conclusions on the bands can be drawn from features called critical points in the $\varepsilon(E)$, which arise from singularities in the joint density of states.[22] We can recognize in Fig. 2 at least four critical points in the measured $\langle\varepsilon(E)\rangle$ spectra. The arrows indicate the positions of these critical points (E_1, E_0, E_0', and E_2).[21] It is also seen that the anodically etched $\langle\varepsilon(E)\rangle$ spectra are quite different from those of the clean, bulk GaP sample. The weakened critical–point natures observed in the anodically etched $\langle\varepsilon(E)\rangle$ spectra indicate considerable roughening of the GaP (100) and (111)*A* surfaces induced by the anodic etching.

To obtain more detailed information on these spectral differences, we solved Fresnel's equation under the assumption of a three-phase (ambient/roughened GaP/bulk GaP) model. An effective-medium approximation (EMA) and a linear regression analysis (LRA) were used for this purpose.[23,24] The EMA deals with the roughened GaP consisting of two constituents, voids (density deficit; $\varepsilon_v=1+i0$) and GaP (ε_c; Ref. 21). We used the Bruggeman EMA defined by the following two equations:[23]

$$f_v\frac{\varepsilon_v-\varepsilon}{\varepsilon_v+2\varepsilon}+f_c\frac{\varepsilon_c-\varepsilon}{\varepsilon_c+2\varepsilon}=0, \tag{1}$$

$$f_v+f_c=1, \tag{2}$$

where f_v and f_c are the volume fractions of the voids and bulk silicon, respectively, and ε is the complex dielectric function of the material investigated.

The dielectric function of an unknown layer or unknown parameters, such as the layer thicknesses and volume fractions of constituent phases, can be numerically determined by minimizing the following mean-squares deviation with a regression program:[24]

$$\sigma^2=\frac{1}{N-P-1}\sum_{j=1}^{N}[(\tan\Psi_j^{\exp}-\tan\Psi_j^{\mathrm{calc}})^2+(\cos\Delta_j^{\exp}-\cos\Delta_j^{\mathrm{calc}})^2], \tag{3}$$

where N is the number of data points and P is the number of unknown model parameters in the analysis. The best-fit model is selected as one that yields a minimum value of σ.

The solid lines in Fig. 5 show the LRA-EMA simulation results for the anodically etched GaP samples. These analyses yield a roughened overlayer thickness of $\sim$5 nm ($\sim$17 nm) and a void fraction of $f_v\sim0.32$(~0.32) with an unbiased estimator of $\sigma=0.057$ (0.277) on the GaP (100) [GaP (111)*A*] surface. It is easily understood from these results that the GaP (111)*A* surface is more roughened than the GaP (100) one. This is in good agreement with those observed in the SEM images, Figs. 1–3. The optical-absorption coefficients for bulk GaP are $\alpha\sim3\times10^5$ cm^{-1} at $E\sim3.5$ eV and $\alpha\sim2\times10^6$ cm^{-1} at $E\sim5$ eV (Ref. 21), respectively. The light penetration depths are then given by $\alpha^{-1}\sim300$ Å ($E\sim3.5$ eV) and ~50 Å ($E\sim5$ eV). These values suggest that the LRA-EMA analyses can account only for the roughened surface of its depth $\leqslant300$ Å. The SE data analysis can also account only for the surface irregularity of its lateral dimension smaller than the light wavelength (~0.25–0.35 μm).[25] No clear difference in the LRA-EMA analyses obtained between the GaP (100) [Figs. 5(a) and 5(b)] and (111)*A* surfaces [Figs. 5(c) and 5(d)] reflect these facts. The large σ value of the GaP (111)*A* surface, however, suggests an invalid assumption of the three-phase model used. We, therefore, reanalyzed the SE data of the GaP (111)*A* surface using the four-phase model. The results obtained were as follows: a roughened overlayer thickness of $d_1\sim13$ nm and a void fraction of $f_{v1}\sim0.36$ on the first roughened overlayer; $d_2\sim21$ nm and $f_{v2}\sim0.12$ on the second roughened overlayer, with an unbiased estimator of $\sigma=0.191$. The four-phase model is, thus, found to slightly improve the fit.

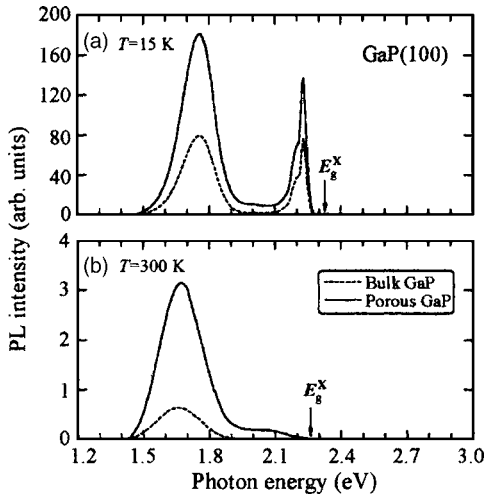

FIG. 6. PL spectra for GaP (100) sample anodically etched in $HF:H_2O_2:C_2H_5OH=1:1:2$ electrolyte for $t=60$ min at constant current of 20 mA/cm^2. The experimental data are taken at $T=15$ and 300 K. For comparison, the PL spectra for clean, bulk GaP are shown by dashed lines. The vertical arrows indicate the positions of the lowest-indirect-band-gap energy E_g^X.[37,38]

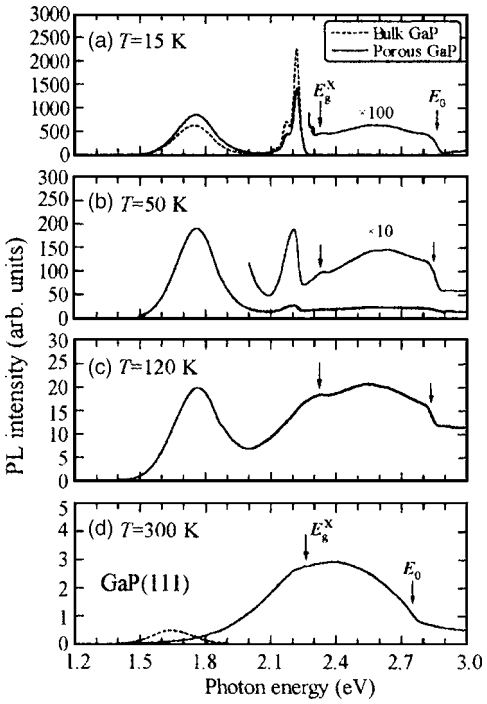

FIG. 7. PL spectra for GaP (111)*A* sample anodically etched in $HF:H_2O_2:C_2H_5OH=1:1:2$ electrolyte for $t=60$ min at constant current of 20 mA/cm^2. The experimental data are taken at $T=14-300$ K. For comparison, the PL spectra for clean, bulk GaP are shown by dashed lines. The vertical arrows indicate the positions of the lowest-indirect-band-gap (E_g^X) and lowest-direct-band-gap energies (E_0).[37,38]

C. Photoluminescence measurement

In order to assess the luminescent properties of porous GaP, we acquired PL spectra at $T=15-300$ K. In Fig. 6, PL spectra for bulk and porous GaP samples formed in $HF:H_2O_2:C_2H_5OH=1:1:2$ electrolyte for $t=60$ min at a constant current of 20 mA/cm^2 are shown. These spectra were obtained at (a) $T=15$ and (b) 300 K. The PL spectrum for the bulk GaP sample at $T=300$ K is dominated by a broad emission band at ~ 1.65 eV. This emission band is attributed to the molecular complexes $Zn_{Ga}-O_P$ and/or $Cd_{Ga}-O_P$ forming an isoelectronic trap in GaP.[26] At $T=15$ K, the bulk GaP sample exhibits, in addition to the broad emission band at ~ 1.75 eV, an intense and narrower emission peak at ~ 2.2 eV. This emission peak is assigned to electron-hole recombination at sulfur-carbon pairs.[26–28] The sulfur-carbon emission peak is found to diminish sharply with increasing temperature and is completely absent at $T>100$ K.

An enhancement of the PL intensity is observed in the porous GaP sample. It is understood from Figs. 6(a) and 6(b) that the PL intensity of the porous GaP sample is about two to four times stronger than for the bulk GaP sample. Photons are detected only if they are emitted in the direction of the detector. The number of such photons should be increased if they are randomly scattered over the surface of a luminescent material. This may be the reason why the PL is more efficiently observed in the porous GaP sample than in the bulk sample. Note that the same phenomenon was reported for porous GaP in Refs. 29–32. On the contrary, a decrease in band-edge emission intensity has been observed in porous GaP,[33] GaAs,[8] InP,[11,34,35] and CdSe.[36] This effect is probably due to the enhanced surface recombination in the porous matrix characterized by a high surface-to-volume ratio.[33,36]

Figure 7 shows the PL spectra for the anodically etched GaP (111)*A* sample in the $HF:H_2O_2:C_2H_5OH=1:1:2$ electrolyte for $t=60$ min at a constant current of 20 mA/cm^2. They were obtained at $T=15-300$ K. For comparison, the PL spectra for the clean, bulk GaP sample obtained at $T=15$ and 300 K are shown by the dashed lines in Figs. 7(a) and 7(d), respectively. The vertical arrows in Figs. 7(a)–7(d) indicate the positions of the lowest-indirect-band-gap (E_g^X) and lowest-direct-band-gap energies (E_0).[37,38]

Similar to the case of the bulk GaP (100) sample (Fig. 6), the PL spectrum for the bulk GaP (111)*A* sample measured at $T=300$ K shows a broad emission band at ~ 1.65 eV, originating from the molecular complexes $Zn_{Ga}-O_P$ and/or $Cd_{Ga}-O_P$, and an additional sharp peak near the E_g^X edge of GaP at $T<100$ K. It is also seen that, in direct contrast to the PL emission from the porous GaP (100) sample shown in Fig. 6, the GaP (111)*A* sample at $T=300$ K shows a strong PL emission in the opaque region, i.e., at energies above ~ 1.8 eV but below E_0 [see Fig. 7(d)]. Note that the PL intensity of the porous GaP (111)*A* sample measured at $T=300$ K is much stronger than that of the bulk sample.

At $T=15$ K, no clear difference can be found in the transparent region ($E<E_g^X$) of the PL spectra between the porous and bulk GaP (111)*A* samples [Fig. 7(a)]. However, a markedly large difference can be found in the opaque region of the PL spectra between these two samples. Although the relative strength is approximately two orders smaller in the opaque region than in the transparent region, the supra-E_g^X component can be clearly detected on the porous GaP (111)*A* sample, but not on the bulk sample. Note that the PL emissions in Fig. 7 are readily visible to the naked eye in (a) green, (b) red, (c) blue, and (d) blue green.

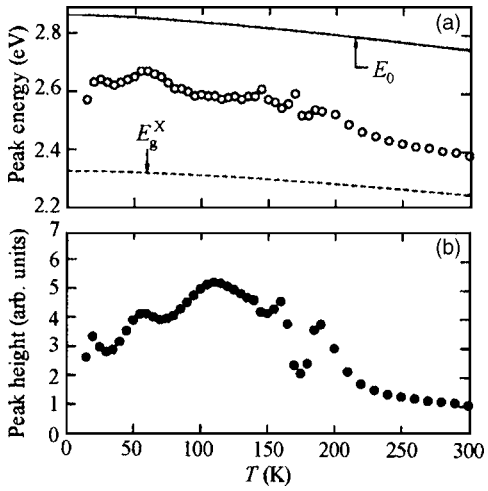

FIG. 8. (a) Peak energy and (b) peak height of supra-E_g^X components vs temperature T for porous GaP (111)A sample anodically etched in $HF:H_2O_2:C_2H_5OH=1:1:2$ electrolyte for $t=60$ min at constant current of 20 mA/cm^2. The temperature variations of E_g^X and E_0 are also plotted in (a) by the dashed and solid lines, respectively.[37,38]

Figure 8 shows a plot of the peak energy and height of the supra-E_g^X component versus temperature T for the porous GaP (111)A sample. The temperature variations of E_g^X and E_0 are also plotted in Fig. 8(a) as dashed and solid lines, respectively. These data were taken from Refs. 37 and 38. The supra-E_g^X emission plotted in Fig. 8(a) has its peak energy falling in the range between E_g^X and E_0. It is also found that the emission intensity exhibits a maximum at $T\sim 110$ K [Fig. 8(b)].

Finally, we schematically show in Fig. 9 the energy-band structure and density-of-states spectrum $N(E)$ for GaP. GaP is an indirect-band-gap semiconductor possessing the zinc-blende structure. The III-V semiconductor material GaP is suitable to study some of the indirect-band-gap effects, since it has three indirect band gaps, $\Gamma_8(\Gamma_{15})\rightarrow X_6(X_1)$ near 2.26 eV, $\Gamma_8(\Gamma_{15})\rightarrow X_7(X_3)$ near 2.48 eV, and $\Gamma_8(\Gamma_{15})\rightarrow L_6(L_1)$ near 2.63 eV, as well as the lowest-direct-band-gap $\Gamma_8(\Gamma_{15})\rightarrow\Gamma_6(\Gamma_1)$ near 2.74 eV, at 300 K.[21,38] The conduction-band (CB) and valence-band (VB) densities of states shown in Fig. 9(b) are represented by the well-known expressions of $N_C\propto(E-E_C)^{1/2}$ and $N_V\propto(E_V-E)^{1/2}$, respectively.

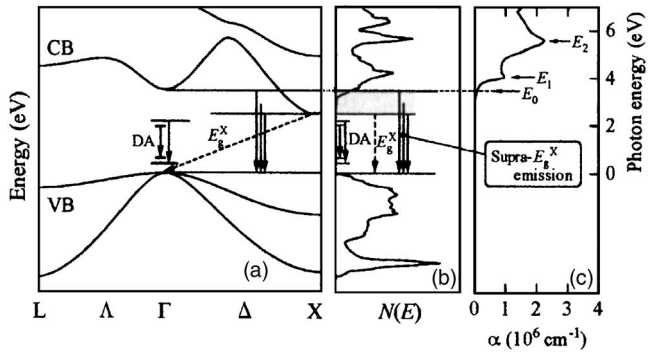

FIG. 9. (a) Schematic energy-band structure and (b) density-of-states spectrum $N(E)$ for GaP. The PL transitions are shown by the vertical arrows. The optical-absorption spectrum $\alpha(E)$ for crystalline GaP is also plotted in (c).[21]

From the deep-level transient spectroscopy and optically detected magnetic resonance in n-GaP,[39,40] the broad emission band peaking at ~1.7 eV has been recently attributed to the radiative recombination of nonequilibrium carriers via donor-acceptor (DA) pairs, the donor being a shallow center. The spectrum dominated near the indirect-band edge of ~2.2 eV at $T=15$ K can be assigned to the DA-pair recombination at sulfur-carbon pairs in bulk GaP and is well known from the literature.[26–28] The DA-pair emissions may be mainly emitted from the surrounding bulk GaP region.

The E_g^X-edge emission has been clearly observed only in the porous GaP (111)A sample as a peak in the experimental PL spectrum at $T=40-140$ K [see Figs. 7(b) and 7(c)]. In view of the experience gained in the study of the luminescence properties of porous silicon, it would be possible to consider that our observed supra-E_g^X emission is the result of quantum size effects in the GaP nanocrystals produced during porous formation. Indeed, an emission peak in the UV spectral region (>3 eV) has ever been observed on porous GaP and has been attributed to the quantum confinement of charged carriers in nanocrystalline GaP.[5,6] Meijerink *et al.*[7] have also observed UV emission in porous GaP but concluded that the emission is due to gallium oxide on the surface of the porous material.

The indirect optical transition process at the indirect-band edge can be expressed as a second-order time-dependent perturbation theory, while that at the direct-band edge is a first-order process.[22] The higher-order process in the indirect-band edge is caused by the requirement of the momentum conservation with emitting and/or absorbing phonons. The indirect optical transition is, therefore, much weaker than the direct one. We consider here that our observed supra-E_g^X emission is due to a nanostructure-induced relaxation of the momentum conservation in the porous GaP layer. The absence of long-range order in an amorphous material renders the Bloch theorem inapplicable and leaves the crystalline momentum $\hbar\mathbf{k}$ undefined. The optical transition in such a case can be described, to a first approximation, by the *nondirect* or, in other words, *quasidirect* transition model in which conservation of the energy but not wave vector is significant.[22,41] Note that the absence of $\mathbf{k}$ space in amorphous materials does not imply that the density of electronic states is not a meaningful concept. The resultant nondirect transition model provides a single, broad absorption peak in optical spectra, which is typically observed in amorphous materials.[21,42] The nanostructured effect considered here is, thus, mainly to enable nondirect optical transition via relaxation of the momentum conservation, rather than enlarging the band gap of the porous GaP layer. In fact, our measured SE spectra do not clearly show the upshift of the band gap in the GaP nanostructures (Fig. 5). The superlattice (SL) is a typical example of a low-dimensional semiconductor material. In GaP/AlP and Si/Ge SLs, the required $\mathbf{k}$ vector can be supplied from the superlattice itself due to the zone-folding effect, and the optical transition occurs without the aid of phonon emission and absorption.

The supra-E_g^X emission observed in Fig. 7 exhibits a steep high-energy end at the E_0 edge. This may be due to the absorption of the emitted light in the surrounding bulk GaP

region. As plotted in Fig. 9(c), the absorption coefficients are $\alpha \sim 20\ \mathrm{cm}^{-1}$ at $E \sim E_g^X (\sim 2.26\ \mathrm{eV})$, $\alpha \sim 1 \times 10^4\ \mathrm{cm}^{-1}$ at $E \sim E_0 (\sim 2.74\ \mathrm{eV})$, and gradually increases with increasing E, reaching a peak value $\alpha \sim 2 \times 10^6\ \mathrm{cm}^{-1}$, at $E \sim E_2 (\sim 5.3\ \mathrm{eV})$.[21] The light penetration depth α^{-1} thus decreases markedly from 500 μm at $E \sim E_g^X$, to 1 μm at $E \sim E_0$, and to 50 Å at $E \sim E_2$. Photons with small diffusive penetration depths for $E > E_0$ can be detected only if they are emitted in the direction of the detector.[43] Photons with very large diffusive penetration depths for $E < E_g^X$ can eventually reach the detector after being internally reflected inside the crystal or at the back surface of the crystal.

No supra-E_g^X luminescence has been observed on the porous GaP (100) sample (Fig. 6). Note that the porous GaP (100) sample has a thin crystalline-GaP surface layer with pits in every spot. The thickness of this layer is approximately 0.5 μm (Fig. 2). Therefore, photons with very large diffusive penetration depths, if they are emitted in the inner porous GaP region, would be strongly absorbed by this surface layer. As a result, only the infra-E_g^X emission, but not the supra-E_g^X emission, has been observed from the porous GaP (100) sample (Fig. 6).

IV. CONCLUSIONS

We studied the structural and optical properties of porous GaP using SEM, SE, and PL spectroscopy. The porous GaP structures were fabricated by electrochemical etching on (100)-oriented and (111)*A*-oriented *n*-GaP substrates in an aqueous electrolyte of $HF:H_2O:C_2H_5OH = 1:1:2$. The SEM images suggested that the morphology of the porous surface is strongly dependent on the substrate orientation. At the beginning of the GaP (100) process, etching started to form pits in the direction vertical to the sample. After initial pitting, further etching proceeded in all directions radially away from the initial etch pit. The GaP (100) surface finally showed a cellular structure with the etch pit as a nucleus, but no further roughening occurred on the surface region.

The pore morphology developed on the GaP (111)*A* surface was quite different from that observed on the GaP (100) surface. No pitting was observed at the beginning of the anodization on the (111)*A* surface. Further anodization led to a (111)*A* surface with a pillar structure characterized by an array of petal-like patterns; each petal-like pattern consists of a lot of columns growing radically and stretching parallel to the (111)*A* surface, resulting in microscopic roughening of the surface. Prolonged anodization led to the formation of a beehivelike porous network inside the sample.

The PL spectra for the porous GaP (100) sample showed only the red emission band at ~1.65 eV at 300 K and the red emission band at ~1.75 eV together with the DA-pair emission at ~2.2 eV at low temperatures. The red and DA-pair emission bands have been typically observed in bulk GaP. Apart from the red emission band, the supra-E_g^X emission has been clearly observed on the porous GaP (111)*A* sample at all temperatures studied ($T = 15-300$ K). The observed supra-E_g^X emission exhibited the steep high-energy end at the E_0 edge. This emission is considered to be due to a nanostructure-induced relaxation of momentum conservation in the porous GaP layer.

[1] L. T. Canham, Appl. Phys. Lett. **57**, 1046 (1990).
[2] A. G. Cullis, L. T. Canham, and P. D. J. Calcott, J. Appl. Phys. **82**, 909 (1997).
[3] L. Canham, *Properties of Porous Silicon* (INSPEC, London, 1997).
[4] S. Ossicini, L. Pavesi, and F. Priolo, *Light Emitting Silicon for Microphotonics* (Springer, Berlin, 2003).
[5] A. Anedda, A. Serpi, V. A. Karavanskii, I. M. Tiginyanu, and V. M. Ichizli, Appl. Phys. Lett. **67**, 3316 (1995).
[6] K. Kuriyama, K. Ushiyama, K. Ohbora, Y. Miyamoto, and S. Kakeda, Phys. Rev. B **58**, 1103 (1998).
[7] A. Meijerink, A. A. Bol, and J. J. Kelly, Appl. Phys. Lett. **69**, 2801 (1996).
[8] P. Schmuki, D. J. Lockwood, H. J. Labbè, and J. W. Fraser, Appl. Phys. Lett. **69**, 1620 (1996).
[9] P. Schmuki, L. E. Erickson, D. J. Lockwood, J. W. Fraser, G. Champion, and H. J. Labbè, Appl. Phys. Lett. **72**, 1039 (1998).
[10] P. Schmuki, L. Santinacci, T. Djenizian, and D. J. Lockwood, Phys. Status Solidi A **182**, 51 (2000).
[11] G. Su, Q. Guo, and R. E. Palmer, J. Appl. Phys. **94**, 7598 (2003).
[12] U. Schlierf, D. J. Lockwood, M. J. Graham, and P. Schmuki, Electrochim. Acta **49**, 1743 (2004).
[13] V. Ichizli, H. L. Hatnagel, H. Mimura, H. Shimawaki, and K. Yokoo, Appl. Phys. Lett. **79**, 4016 (2001).
[14] V. N. Tondare, M. Naddaf, A. B. Bhise, S. V. Bhoraskar, D. S. Joag, A. B. Mandale, and S. R. Sainkar, Appl. Phys. Lett. **80**, 1085 (2002).
[15] I. M. Tiginyanu, I. V. Kravetsky, S. Langa, G. Marowsky, J. Monecke, and H. Föll, Phys. Status Solidi A **197**, 549 (2003).
[16] M. Christophersen, J. Carstensen, S. Rönnebeck, C. Jäger, W. Jäger, and H. Föll, J. Electrochem. Soc. **148**, E267 (2001).
[17] B. H. Erné, D. Vanmaekelbergh, and J. J. Kelly, J. Electrochem. Soc. **143**, 305 (1996).
[18] R. W. Tjerkstra, J. Gómez Rivas, D. Vanmaekelbergh, and J. J. Kelly, Electrochem. Solid-State Lett. **5**, G32 (2002).
[19] T. Smith, J. Opt. Soc. Am. **58**, 1069 (1968).
[20] S. Anderieu and F. A. d'Avitaya, Surf. Sci. **219**, 277 (1989).
[21] S. Adachi, *Optical Constants of Crystalline and Amorphous Semiconductors: Numerical Data and Graphical Information* (Kluwer Academic, Boston, 1999).
[22] S. Adachi, *Optical Properties of Crystalline and Amorphous Semiconductors: Materials and Fundamental Principles* (Kluwer Academic, Boston, 1999).
[23] D. E. Aspnes, J. B. Theeten, and F. Hottier, Phys. Rev. B **20**, 3292 (1979).
[24] R. M. A. Azzam and N. M. Bashara, *Ellipsometry and Polarized Light* (North-Holland, Amsterdam, 1977).
[25] K. Sakaino and S. Adachi, J. Electrochem. Soc. **149**, G543 (2002).
[26] A. N. Pikhtin and O. L. Lazarenkova, in *Handbook of Electroluminescent Materials*, edited by D. R. Vij (Institute of Physics Publishing, Bristol, 2004), p. 282.
[27] P. J. Dean, C. J. Frosch, and C. H. Henry, J. Appl. Phys. **39**, 5631 (1968).
[28] P. J. Dean, J. D. Cuthbert, and R. T. Lynch, Phys. Rev. **179**, 754 (1969).
[29] A. I. Belogorokhov, V. A. Karavanskiĭ, A. N. Obraztsov, and V. Y. Timoshenko, JETP Lett. **60**, 274 (1994).
[30] A. V. Zoteev, P. K. Kashkarov, A. N. Obraztsov, and V. Y. Timoshenko, Semiconductors **30**, 775 (1996).
[31] A. A. Lebedev, V. Y. Rud', and Y. V. Rud', Tech. Phys. Lett. **22**, 754 (1996).
[32] M. A. Stevens-Kalceff, I. M. Tiginyanu, S. Langa, H. Föll, and H. L. Hartnagel, J. Appl. Phys. **89**, 2560 (2001).
[33] M. A. Stevens-Kalceff, S. Langa, I. M. Tiginyanu, J. Carstensen, M. Christophersen, and H. Föll, Mater. Res. Soc. Symp. Proc. **638**, F5.31.1 (2001).
[34] T. Takizawa, S. Arai, and M. Nakahara, Jpn. J. Appl. Phys., Part 2 **33**, L643 (1994).
[35] A. Liu and C. Duan, Appl. Phys. Lett. **78**, 43 (2001).
[36] I. M. Tiginyanu, E. Monaico, V. V. Ursaki, V. E. Tezlevan, and R. W. Boyd, Appl. Phys. Lett. **86**, 063115 (2005).
[37] S. Adachi, *Properties of Group-IV, III–V and II–VI Semiconductors* (Wiley, Chichester, 2005).
[38] S. Adachi, *Handbook on Physical Properties of Semiconductors: III–V*

Compound Semiconductors (Kluwer Academic, Boston, 2004) Vol. 2.
[39]Y. Ishikawa, Y. Hayashi, and N. Itoh, J. Appl. Phys. **65**, 2035 (1989).
[40]O. O. Awadelkarim, M. Godlewski, and B. Monemar, Mater. Sci. Forum **38–41**, 821 (1989).
[41]D. T. Pierce and W. E. Spicer, Phys. Rev. B **5**, 3017 (1972).
[42]J. Tauc, in *Amorphous and Liquid Semiconductors*, edited by J. Tauc (Plenum, London, 1974), p. 159.
[43]A. F. van Driel, B. P. J. Bret, D. Vanmaekelbergh, and J. J. Kelly, Surf. Sci. **529**, 197 (2003).